THE JOURNAL OF PHYSICAL CHEMISTRY B
A JOURNAL OF THE AMERICAN CHEMICAL SOCIETY

pubs.acs.org/JPCB

Article

Does Viscosity Drive the Dynamics in an Alcohol-Based Deep Eutectic Solvent?

Srijan Chatterjee,* Samadhan H. Deshmukh, and Sayan Bagchi*

Cite This: J. Phys. Chem. B 2022, 126, 8331−8337

Read Online

ACCESS | Metrics & More | Article Recommendations | Supporting Information

ABSTRACT: Deep eutectic solvents, consisting of heterogeneous nanodomains of hydrogen-bonded networks, have evolved into a range of viscous fluids that find applications in several fields. As viscosity is known to influence the dynamics of other neoteric solvents like ionic liquids, understanding the effect of viscosity on deep eutectic solvents is crucial to realize their full potential. Herein, we combine polarization-selective pump−probe spectroscopy, two-dimensional infrared spectroscopy, and molecular dynamics simulations to elucidate the impact of viscosity on the dynamics of an alcohol-based deep eutectic solvent, ethaline. We compare the solvent fluctuation and solute reorientation time scales in ethaline with those in ethylene glycol, an ethaline constituent. Interestingly, we find that the solute's reorientation apparently scales the bulk viscosity of the solvent, but the same is not valid for the overall solvation dynamics. Using the variations in the estimated intercomponent hydrogen bond lifetimes, we show that a dissolved solute does not sense the bulk viscosity of the deep eutectic solvent; instead, it senses domain-specific local viscosity determined by the making and breaking of the hydrogen bond network. Our results indicate that understanding the domain-specific local environment experienced by the dissolved solute is of utmost importance in deep eutectic solvents.

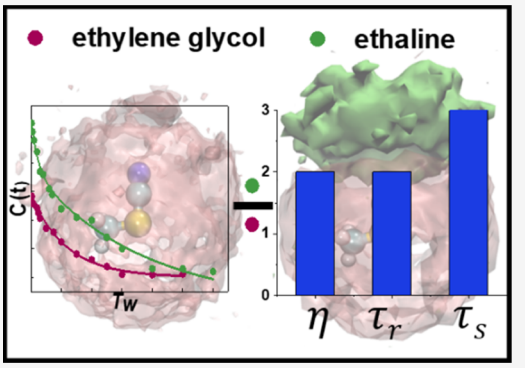

INTRODUCTION

Over the last two decades, deep eutectic solvents (DESs) have emerged as promising green alternatives to conventional solvents due to their favorable properties, such as biodegradability, low vapor pressure, high conductivity, and recyclability.[1−6] Unlike homogeneous molecular solvents, DESs usually consist of two components, a hydrogen bond donor (HBD) and a hydrogen bond acceptor (HBA), such that the melting temperature (T_m) of the mixture is lower than the T_m of the pure components.[7−9] The recent interest in DESs stems from the opportunity of modulating their solvating properties by changing their chemical composition.[10,11] DESs have wide-range applications as sustainable media in extractions, analysis, organic synthesis, electrochemistry, electrodeposition, biocatalysis, and nanomaterial synthesis and processing.[1,6,12−14]

DES formation has been ascribed to the intercomponent hydrogen bonds (HBs) between the HBA and the HBD.[8,10,15−17] A reported drawback of DESs is their high viscosity, which limits their application potential.[11,18,19] Despite the well-documented influence of viscosity on the dynamics in other neoteric solvents (e.g., ionic liquids), the effect of viscosity on the DES dynamics is primarily unexplored.[20−22] Due to the diverse intermolecular interactions within DES components, the formation of heterogeneous nanostructures in a DES has been reported.[23,24] Although bulk viscosity has been measured for different deep eutectic systems, it is highly unlikely that uniform viscosity is maintained across the heterogeneous nanostructures. It is still unknown if a solute dissolved in a DES nanodomain would sense the bulk DES viscosity or domain-specific effective viscosity. In addition, previous studies primarily focused on understanding the DES characteristics without any dissolved solute.[18,25,26] As DESs are relatively recent constructs with applications in several fields, understanding the dependence of the dynamics on viscosity, from the perspective of both the solute and the solvent, is required to realize their full potential.

Herein, we report the viscosity dependence of solvent fluctuations and solute reorientation in a deep eutectic solvent using two-dimensional infrared (2D IR) spectroscopy[21,27,28] and polarization-selective pump−probe (PSPP) spectroscopy.[29] Some of the recent 2D IR reports on DESs have focused on comparing the solvation dynamics among different DES families.[30,31] However, the effect of the domain-specific viscosity experienced by a small solute is mostly unexplored. Due to the long vibrational lifetime of the nitrile stretch,[32] we choose methyl thiocyanate (MeSCN, solute) as the vibrational

Received: September 12, 2022
Published: October 6, 2022

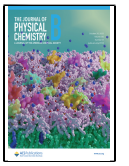

https://doi.org/10.1021/acs.jpcb.2c06521
J. Phys. Chem. B 2022, 126, 8331−8337

reporter of the viscous environment. Although most eutectic mixtures contain high-melting-point solid components, ethaline, a 2:1 molar mixture of ethylene glycol (EG, HBD) and choline chloride (HBA), is unique, as EG is liquid at room temperature. Interestingly, EG can act as both HBA and HBD to form an intricate hydrogen bond network of its own, resulting in alcohol clusters of various sizes.[33,34] The distinct difference in the viscosities (η) of ethaline and neat EG at room temperature (η_{EG} = 17 cP, $\eta_{ethaline}$ = 36 cP)[19,35] allows us to illustrate the role of intercomponent friction in DES dynamics. We also perform molecular dynamics (MD) simulations to estimate the intercomponent HB lifetimes. While the experiments allow us to compare the solvation structure and dynamics, MD simulations permit us to decipher the dependence of the solute's reorientation on the domain-specific local viscosity.

MATERIALS

Choline chloride (ChCl, >98.9%), methyl thiocyante (MeSCN, >99.9%), and ethylene glycol (EG, >99.8%) were purchased from Sigma-Aldrich, and except for ChCl, others were used without further purification.

DES Synthesis. Ethaline DES was prepared according to the previously mentioned procedure.[1] To start with, ChCl was dried in a vacuum oven overnight at 90 °C to remove any water impurity. DES synthesis was performed in an argon-filled glovebox and the prepared DES was found to have negligible water content with the help of a Karl Fischer titrator.

FTIR Spectroscopy. FTIR spectra were recorded in a Bruker Vertex 70 FTIR spectrometer with a demountable cell consisting of two CaF_2 windows (3 mm thickness) separated by a 100 μm Mylar Spacer. MeSCN was added into the EG and ethaline solutions such that the final concentration reached ~100 mM. 2D IR experiments were performed using the same solution as FTIR, with the same sample cell. Reported FTIR peak positions were obtained by fitting the experimental IR spectra with Voigt line shape functions.

2D IR Spectroscopy. 2D IR and PSPP spectra were acquired using a pulse shaper-based 2D IR spectrometer designed by PhaseTech spectroscopy, Inc. A detailed description of the 2D IR setup is mentioned previously. Briefly, 800 nm output from a Ti−sapphire amplifier was converted to a mid-IR beam centered at ~2160 cm^{-1} with a ~60 fs pulse width by an optical parametric amplifier (OPA, OPerA Solo, Coherent). This IR pulse was then divided into a strong excitation pulse (80%) and a weak detection pulse (20%) using a beam splitter. A germanium acoustic-optic modulator (AOM)-based pulse shaper shaped the pump pulses and created the initial coherence period (τ). Excitation and detection pulses were spatially overlapped and focused onto the sample cell using parabolic mirrors. τ was scanned to generate the 2D IR signal at a fixed temporal delay (waiting time, T_w) between the excitation and detection pulses. The signal was dispersed with a monochromator (Princeton Instruments) and detected using a nitrogen-cooled 64-pixel HgCdTe (MCT) IR array (InfraRed Associates) detector. The 2D IR experimental data at a fixed T_w were a function of the variable delay time between the two excitation pulses (τ) and detection frequencies. Numerical Fourier transform provided the second frequency variable, excitation frequencies. A 2D spectrum was obtained for each waiting time, T_w.

Waiting-time-dependent evolution of the 2D IR line shapes, i.e., spectral diffusion $C(t)$, was analyzed using the center line slope (CLS) method.[36] The CLS decay curves were fitted with the following biexponential functions to extract the time constants

$$C(t) = \sum_{i=1}^{2} a_i e^{(t/\tau_i)}$$

PSPP Spectroscopy. Polarization-selective pump−probe experiments were performed to obtain the pump−probe signals in the parallel $\langle XXXX \rangle$ and perpendicular $\langle XXYY \rangle$ polarization conditions. The polarization of the pump beam was either parallel or perpendicular with respect to that of the probe beam. Pump polarization before the sample was controlled using the combination of a quarter-wave plate and a polarizer.

Parallel $I_{\parallel}(t)$ and perpendicular $I_{\perp}(t)$ signals can be expressed using the following equations

$$I_{\parallel}(t) = P(t)[1 + 0.8C_2(t)] \quad (1)$$

$$I_{\perp}(t) = P(t)[1 - 0.4C_2(t)] \quad (2)$$

where $P(t)$ is the isotropic pump−probe decay and $C_2(t)$ is the second-order Legendre polynomial orientation correlation function of the transition dipole moment.

By rearranging eqs 1 and 2, we obtain

$$[I_{\parallel}(t) + 2I_{\perp}(t)] = 3P(t) \quad (3)$$

$$[I_{\parallel}(t) - I_{\perp}(t)] = 1.2P(t)C_2(t) \quad (4)$$

Orientational anisotropy $r(t)$ can subsequently be obtained from eqs 3 and 4

$$r(t) = \frac{I_{\parallel}(t) - I_{\perp}(t)}{I_{\parallel}(t) + 2I_{\perp}(t)} = 0.4\, C_2(t) \quad (5)$$

$r(t)$ in eq 5 is a ratio of the LHSs of eqs 4 and 3. As $[I_{\parallel}(t) + 2I_{\perp}(t)]$ and $[I_{\parallel}(t) - I_{\perp}(t)]$ decay over time, dividing one small number (~0) by another (~0) at large pump−probe delays would incorporate a large error in the anisotropy value. To eliminate the error, we have simultaneously fitted $[I_{\parallel}(t) + 2I_{\perp}(t)]$ and $[I_{\parallel}(t) - I_{\perp}(t)]$ using multiexponential decay functions for $P(t)$ and single-exponential decay for $C_2(t)$, such that the same decay corresponding to $P(t)$ fits both $[I_{\parallel}(t) + 2I_{\perp}(t)]$ and $[I_{\parallel}(t) - I_{\perp}(t)]$. This method, by far, provides significantly better results than direct fitting of $r(t)$. The anisotropy $r(t)$ obtained from the fits shows an excellent agreement with experimentally obtained anisotropies.

MD Simulations. All-atom classical MD simulations of MeSCN in the EG and ethaline system were performed in the GROMACS 2021 package.[37] Force field parameters for EG and ethaline were taken from the work of Doherty et al.[38] GAFF force field parameterization with antechamber suits was used for MeSCN.[39] A simulation box was constructed using a MeSCN molecule and a molar ratio of choline chloride and EG of 1:2 for the ethaline DES simulation. The system was first energy-minimized with the steepest decent algorithm with a 2 fs step size. Further, it was equilibrated in a velocity rescale thermostat at 300 K for 1 ns and a Parrinello−Rahman barostat at 300 K and 1 bar for 5 ns. Production runs were calculated for a further 100 ns. Hydrogen bond analysis with lifetime calculations was performed using a GROMACS analysis tool, gmx hbond, with default criteria. A three-

https://doi.org/10.1021/acs.jpcb.2c06521
J. Phys. Chem. B 2022, 126, 8331−8337

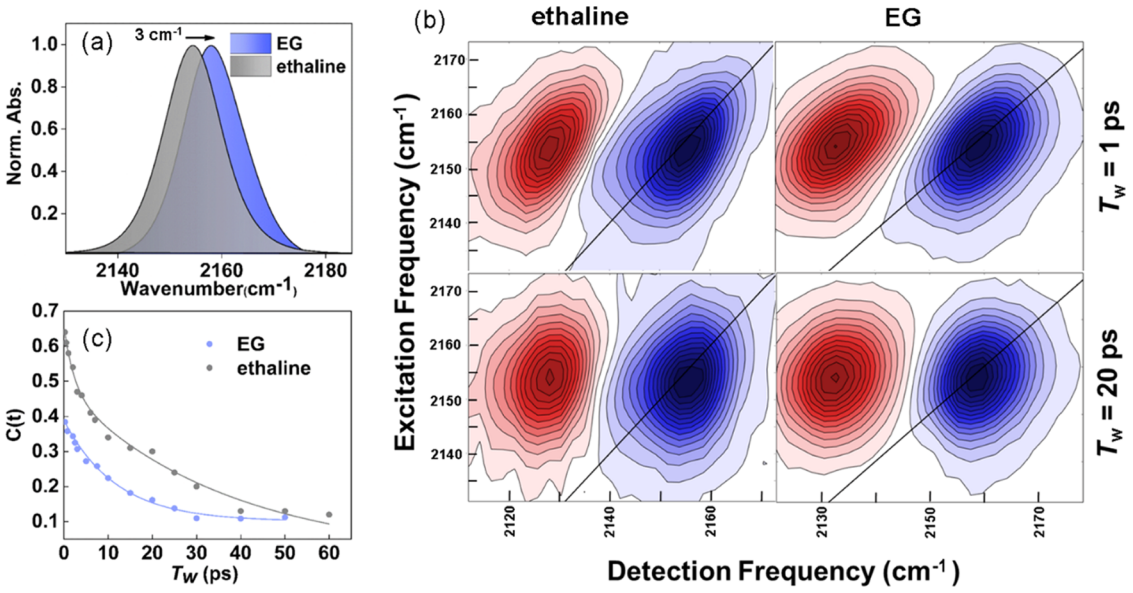

Figure 1. (a) FTIR spectra of the CN stretch of MeSCN in ethaline and EG. The CN absorption shows a 3 cm^{-1} blue shift in EG compared to that in ethaline. The full width at half-maximum (FWHM) of the CN stretch spectrum is the same in both solvents. (b) 2D IR spectra of the CN stretch of MeSCN in ethaline (left panels) and EG (right panels). The top and bottom panels correspond to T_w = 1 ps and T_w = 20 ps, respectively. (c) Frequency−frequency correlation function $C(t)$ decay curves of MeSCN at a function of T_w in EG and ethaline. The decay curves indicate that the solvent fluctuation is slower in ethaline than that in EG.

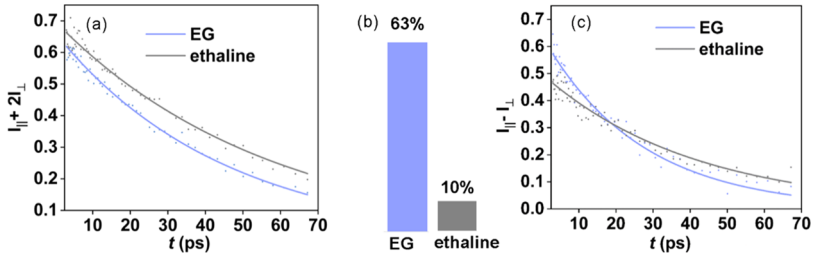

Figure 2. Results from polarization-selective pump−probe experiments and HB analysis from MD simulation trajectories. (a) The decay of the ($I_{\parallel}$ + $2I_{\perp}$) signal of the CN stretch as a function of time in EG and ethaline. (b) HB population MeSCN in EG and ethaline obtained from MD simulations. The vibrational probe experiences considerably more HB population in EG than that in ethaline, indicating a change in the solvation environment in the two solvents. (c) The decay of the ($I_{\parallel} - I_{\perp}$) signal of the CN stretch as a function of time in EG and ethaline. Simultaneous fitting of ($I_{\parallel}$ + $2I_{\perp}$) and ($I_{\parallel} - I_{\perp}$) decays was performed to obtain the anisotropy $r(t)$ decay, which is given by the expression $r(t) = \frac{I_{\parallel} - I_{\perp}}{I_{\parallel} + 2I_{\perp}} = 0.4C_2(t)$.

dimensional spatial distribution plot was obtained using the TRAVIS package.[40]

RESULTS AND DISCUSSION

The IR absorption spectra of the CN stretch show a symmetric peak in ethaline and EG (Figure 1a). Although Figure 1a shows symmetric peaks, various subensembles exist within the absorption bands due to the heterogeneity in the solvent configurations that determine CN's frequency through intermolecular interactions.[41] As the solvent structures evolve over time, these subensembles exchange on the time scales of the solvent fluctuations, making the probe transition frequency (ω) fluctuate from its average $\langle\omega\rangle$. 2D IR spectroscopy allows direct extraction of the frequency−frequency correlation function ($C(t) = \langle\delta\omega(t)\delta\omega(0)\rangle$) of a vibrational transition, where $\delta\omega = \omega(t) - \langle\omega\rangle$ is the time-dependent fluctuation.[36,42,43] The 2D IR spectra (Figure 1b) are elongated along the diagonal at early time delays (T_w), indicating that the excitation and detection frequencies are correlated. At longer T_w, the correlations are lost due to solvent fluctuations, and the spectra become circular. The analysis of the 2D IR spectral shapes as a function of T_w provides the decay of $C(t)$, referred to as spectral diffusion.

Figure 1c shows the $C(t)$ of the CN peak in EG and ethaline. In both solvents, $C(t)$ fits to biexponential functions (Table S1). The faster time constants, related to the local solvent fluctuations around the solute, are the same for ethaline and EG within the experimental error. However, the slower time constant (τ_s), related to the bulk dynamics of the solvent, slows down considerably going from EG (~12 ps) to ethaline (~39 ps). The estimated slow time constants indicate retardation of the solvent dynamics with an increase in viscosity. Interestingly, the time scales demonstrate that a 2-fold increase in viscosity results in a nearly 3-fold slowdown of the spectral diffusion. Our results illustrate that adding choline chloride increases the solvent inhomogeneity, as evidenced by the $C(t)$ value in ethaline at T_w = 0, relative to that in EG (see the last column of Table S1). In the absence of any motionally narrowed homogeneous dynamics, $C(t)$ at T_w = 0 should be unity.[20,44] The smaller initial drop in ethaline demonstrates

https://doi.org/10.1021/acs.jpcb.2c06521
J. Phys. Chem. B 2022, 126, 8331−8337

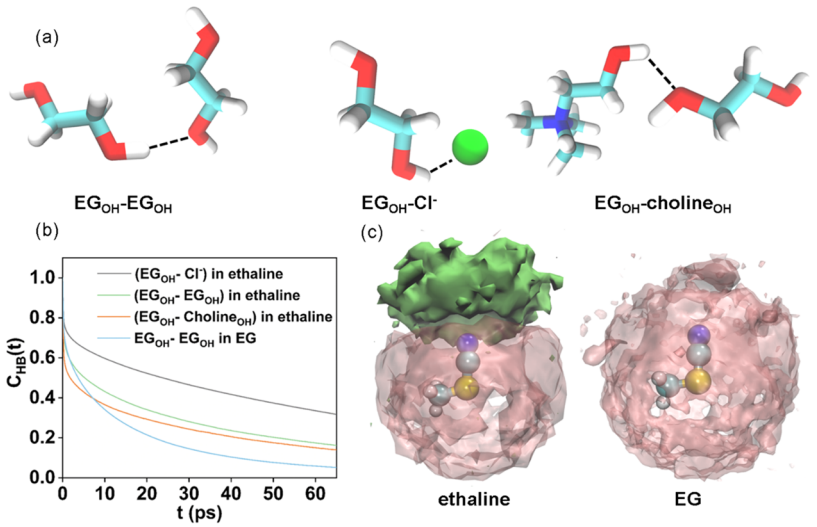

Figure 3. (a) Schematic diagrams of the three possible HB scenarios in ethaline. In EG, $EG_{OH}-EG_{OH}$ HB is the only possibility. (b) Lifetime decays of different HB types in EG and ethaline. (c) Spatial distribution functions of choline(green) and EG (pink) around MeSCN in ethaline (left) and EG (right).

larger inhomogeneity arising from the disruption of the extended alcohol HB network by choline chloride.

The solute reorientation is estimated from the PSPP experiments. Before we discuss the solute reorientation, it is interesting to note that the vibrational lifetime is faster in EG than that in ethaline (Figure 2a). The faster vibrational lifetime contributes to larger homogeneous dynamics and agrees well with the larger initial drop from unity (Figure 1c). A faster lifetime is known to arise from the formation of a solute−solvent HB. The ∼3 cm^{-1} blue shift in peak maxima going from ethaline to EG (Figure 1a) and previous reports of negligible HB of MeSCN in ethaline indicate considerably more HBs between the probe and the OH moieties in EG. In agreement with our experimental results, the HB analysis of the MD simulation trajectories predicts an increase in the HB propensity of the solute going from the DES to EG (Figure 2b). HB is generally associated with the broadening of the IR absorption peak. However, we observe that the peaks in EG and ethaline have the same full width at half-maximum (FWHM) of ∼13.5 cm^{-1} (Figure 1a) despite the change in HB propensity. The FWHM is expected to be larger in EG than that in ethaline due to the predominance of the solute−EG_{OH} HB conformations in EG. However, a motionally narrowed homogeneous component in EG, arising from ultrafast solute motions, plausibly cancels out the increase in the FWHM.

The anisotropy $r(t)$ is obtained from PSPP experiments performed at parallel ($I_{\|}$) and perpendicular ($I_{\perp}$) polarization conditions. $r(t)$ provides the orientational dynamics through the expression $r(t) = \frac{I_{\|} - I_{\perp}}{I_{\|} + 2I_{\perp}} = 0.4C_2(t)$, where $C_2(t)$ is the second-order Legendre polynomial orientational correlation function. We obtain $r(t)$ by simultaneously fitting the difference ($I_{\|} - I_{\perp}$; Figure 2c) and the sum ($I_{\|} + 2I_{\perp}$; Figure 2a, see PSPP Spectroscopy section for more details). The anisotropy decays in EG and ethaline fit to single-exponential functions where the time constant t_r (Table S2) provides the time scales for complete randomization. The randomization time scale, related to the free orientational diffusion constant ($D_m = 1/6t_r$), shows a nearly 2-fold slowdown in the rotational diffusion of the solute going from EG to ethaline.

The time constant t_r can be compared to the predictions of rotational diffusion in the hydrodynamic limit, using a modified Debye−Stokes−Einstein equation. If the diffusive motion is well-described by hydrodynamics, the orientational relaxation time can be related to the properties of the system by $t_r = fV_{eff}\eta/k_BT$.[21] Here, T is the absolute temperature, η is the solvent viscosity, k_B is Boltzmann's constant, f is the shape factor, and V_{eff} is the effective molecular volume.

We estimate the dimensions of the solute molecule using the known bond lengths and the van der Waals radii of the atoms. As the size of the solute is either smaller or comparable to that of the solvent, slip boundary conditions are a reasonable model for the solute's reorientation dynamics. Slip boundary conditions are applied when the friction opposing reorientation arises from the solvent in the swept volume of the solute.[21] Considering the axial ratios of the MeSCN spheroid, f is obtained from the calculations by Youngren et al.[45] and Hu et al.[46] Calculated t_r^{slip} values are provided in Table S2 next to the measured t_r values. The measured and calculated time constants in ethaline and EG show excellent agreement. Therefore, the 2-fold retardation observed in the measured reorientation dynamics indicates that DES viscosity predominantly dictates the solute's rotational diffusion.

It is intriguing to note that although solute dynamics scales with viscosity, the solvent fluctuations show a larger slowdown than that predicted from viscosity. To understand this phenomenon, we have analyzed the lifetimes of the different intercomponent HBs in ethaline. As multiple HB partners are present in the DES, the overall solvent fluctuation should depend on the making and breaking of all of the individual intercomponent HBs ($EG_{OH}-EG_{OH}$, EG_{OH}−choline$_{OH}$, and $EG_{OH}-Cl^-$; Figure 3a). Figure 3b shows the HB lifetime autocorrelation functions ($C_{HB}(t)$) in ethaline between EG and other HB partners. Triexponential fits to $C_{HB}(t)$ show two fast time scales (similar in all cases, within the fitting error) plausibly arising from librational motions and the HB making/breaking between the same pair of solvent molecules and a component-specific slower time scale (Table S3). Our computational results suggest that the $C_{HB}(t)$ of the $EG_{OH}-EG_{OH}$ HB dynamics scales the bulk viscosity. The $C_{HB}(t)$ of

https://doi.org/10.1021/acs.jpcb.2c06521
J. Phys. Chem. B 2022, 126, 8331−8337

EG_{OH}–EG_{OH} is slower in the DES by almost a factor of 2 than that in EG. Within the different intercomponent HB of ethaline, $C_{HB}(t)$ is the slowest for the EG_{OH}–Cl^- HB, while the lifetimes of the EG_{OH}–EG_{OH} and EG_{OH}–$choline_{OH}$ HBs are comparable.

If we assume a similar solvation environment, the retardation in solute reorientation can be explained based on the slowdown of the EG_{OH}–EG_{OH} HB lifetimes in ethaline and EG. However, the spatial density functions (SDFs, Figure 3c) indicate an altered environment where the choline component of the DES preferentially interacts with the solute nitrogen. Therefore, the complete reorientation of the solute molecule will need rearrangement of both the EG_{OH}–EG_{OH} and EG_{OH}–$choline_{OH}$ HBs. Since the estimated HB lifetimes of EG_{OH}–EG_{OH} and EG_{OH}–$choline_{OH}$ HBs are the same, the solute reorientation scales the EG_{OH}–EG_{OH} HB lifetimes in both environments. On the other hand, DESs have been reported to form heterogeneous nanodomains.[47] The fluctuation time scale of each domain depends on the intercomponent HB prevalent in the domain. Our experimental results can be rationalized if we consider that the solute only experiences the local friction of the domain in which it is located. Even though the presence of more viscous domains can slow down the randomization of the total liquid structure by restricting the motions of the less viscous regions, they do not completely determine the friction felt locally by MeSCN. The agreement between measured and predicted t_r values (Table S2) indicates that the domain-specific local viscosity experienced by the solute is the same as the reported bulk viscosity of ethaline. As spectral diffusion measures the overall evolution of the solvent structures in all of the domains, the presence of much slower HB dynamics (EG_{OH}–Cl^-) does not allow the spectral diffusion to mirror the bulk viscosity changes. To this end, comparing the viscosity dependence of the solute reorientation and the solvent fluctuation dynamics in various DESs can provide an interesting perspective to tailor DESs for specific applications.

However, the apparent correlation between the solute reorientation time scale and the overall solvent viscosity exists because of two reasons: (1) the local microviscosity around MeSCN mirrors the bulk viscosity of ethaline, and (2) the HB lifetimes of the ethaline DES components solvating MeSCN, EG_{OH}–EG_{OH} and EG_{OH}–$choline_{OH}$, are the same. However, dynamic heterogeneity has been previously reported as an important characteristic of DESs, resulting in the fractional dependence of the solute reorientation time scale on viscosity.[23] A previous report on a nonionic DES predicts that depending on the structure and the intermolecular interactions of the probe, it would selectively reside in a specific nanodomain of the heterogeneous DES.[31] As ethaline DES is also heterogeneous,[48,49] there could indeed be a scenario where a solute would be located in a different domain. Interestingly, another report on an ionic probe in ethaline (unlike the neutral probe reported here) predicts a much broader FWHM compared to our results, indicating different domain selections.[30] The previous report on the ionic probe also showed a much broader asymmetric peak shape in EG compared to DES, which is not evident in our case. The previous report compared the solvation dynamics and their relation to the bulk viscosities across DES families; however, the reorientation dynamics of the ionic solute was not reported.[30] Thus, although the previous results are complementary to our findings, a direct comparison between the two studies is not possible to elucidate the effect of the domain-specific viscosity on an ionic solute and a neutral solute.

Another important aspect to decipher the origin of the local viscosity is to look into different intercomponent HB lifetimes. To the best of our knowledge, this is the first study where experimental understanding of ultrafast solvation dynamics and reorientation dynamics in DES have been directly correlated to the theoretical calculations of HB lifetimes using MD simulations. When a solute selects a particular nanodomain, its reorientation in this nanodomainis generally governed by the rearrangement of a different intercomponent HB. As a different HB might have a different lifetime, the reorientation time scale can be different. The time scale will depend on the steric and electrostatic stabilization of the solute by the DES components, leading to the preferential selection of the domain.

CONCLUSIONS

In this study, we used time-resolved vibrational spectroscopies to estimate the time scales of the solvent fluctuation and the reorientation dynamics of a small neutral solute dissolved in a DES, ethaline. We compared the time scales with those observed in EG, an ethaline component, which can act as both HBA and HBD. Our results show that increased solvent viscosity slows down the spectral diffusion of the solute. The spectral diffusion time scale increases by a factor of 3 (slower), while the viscosity increases by a factor of 2. Unlike the spectral diffusion time scales, the estimated solute reorientation time scales apparently scale the bulk viscosity of the solvent. MD-estimated time scales of the intercomponent HB dynamics reveal that the solute does not sense the bulk viscosity; instead, it senses the domain-specific microviscosity determined by the making and breaking of the interspecies hydrogen bond network. This insight is particularly exciting because a large body of recent studies indicates that the microheterogeneity in DES still lacks fundamental understanding. Interestingly, this article shows that the combination of 2D IR, PSPP, and MD simulations is capable to identify the viscosity dependence of the domain-specific dynamics experienced by the probe in heterogeneous systems like DESs. How local interactions of the probe determines the domain specificity would be explored in detail in future work.

ASSOCIATED CONTENT

Supporting Information

The Supporting Information is available free of charge at https://pubs.acs.org/doi/10.1021/acs.jpcb.2c06521.

Tables for correlation function decays (PDF)

AUTHOR INFORMATION

Corresponding Authors

Srijan Chatterjee – *Physical and Materials Chemistry Division, National Chemical Laboratory (CSIR-NCL), Pune 411008, India; Academy of Scientific and Innovative Research (AcSIR), Ghaziabad 201002, India;* orcid.org/0000-0001-9701-4158; Email: srijan9x@gmail.com

Sayan Bagchi – *Physical and Materials Chemistry Division, National Chemical Laboratory (CSIR-NCL), Pune 411008, India; Academy of Scientific and Innovative Research (AcSIR), Ghaziabad 201002, India;* orcid.org/0000-0001-6932-3113; Email: s.bagchi@ncl.res.in

https://doi.org/10.1021/acs.jpcb.2c06521
J. Phys. Chem. B 2022, 126, 8331–8337

Author

Samadhan H. Deshmukh − *Physical and Materials Chemistry Division, National Chemical Laboratory (CSIR-NCL), Pune 411008, India; Academy of Scientific and Innovative Research (AcSIR), Ghaziabad 201002, India;* orcid.org/0000-0002-0326-6125

Complete contact information is available at: https://pubs.acs.org/10.1021/acs.jpcb.2c06521

Notes

The authors declare no competing financial interest.

■ ACKNOWLEDGMENTS

S.B. acknowledges CSIR-NCL and SERB, India (EMR/2016/000576), for financial support. The authors acknowledge the computational facilities at CSIR-NCL. The authors also acknowledge the National Supercomputing Mission (NSM) for providing computing resources of "PARAM Brahma" at IISER Pune, which is implemented by C-DAC and supported by the Ministry of Electronics and Information Technology (MeitY) and Department of Science and Technology (DST), Government of India. S.H.D. acknowledges CSIR for research fellowship.

■ REFERENCES

(1) Smith, E. L.; Abbott, A. P.; Ryder, K. S. Deep Eutectic Solvents (DESs) and Their Applications. *Chem. Rev.* **2014**, *114*, 11060−11082.

(2) Abbott, A. P.; Capper, G.; Davies, D. L.; Rasheed, R. K.; Tambyrajah, V. Novel solvent properties of choline chloride/urea mixtures. *ChemComm* **2003**, 70−71.

(3) Abbott, A. P.; Boothby, D.; Capper, G.; Davies, D. L.; Rasheed, R. K. Deep Eutectic Solvents Formed between Choline Chloride and Carboxylic Acids: Versatile Alternatives to Ionic Liquids. *J. Am. Chem. Soc.* **2004**, *126*, 9142−9147.

(4) Zhang, Q.; De Oliveira Vigier, K.; Royer, S.; Jerome, F. Deep eutectic solvents: syntheses, properties and applications. *Chem. Soc. Rev.* **2012**, *41*, 7108−7146.

(5) Ge, X.; Gu, C.; Wang, X.; Tu, J. Deep eutectic solvents (DESs)-derived advanced functional materials for energy and environmental applications: challenges, opportunities, and future vision. *J. Mater. Chem. A* **2017**, *5*, 8209−8229.

(6) Hansen, B. B.; Spittle, S.; Chen, B.; Poe, D.; Zhang, Y.; Klein, J. M.; Horton, A.; Adhikari, L.; Zelovich, T.; Doherty, B. W.; Gurkan, B.; Maginn, E. J.; Ragauskas, A.; Dadmun, M.; Zawodzinski, T. A.; Baker, G. A.; Tuckerman, M. E.; Savinell, R. F.; Sangoro, J. R. Deep Eutectic Solvents: A Review of Fundamentals and Applications. *Chem. Rev.* **2021**, *121*, 1232−1285.

(7) Zhang, Y.; Poe, D.; Heroux, L.; Squire, H.; Doherty, B. W.; Long, Z.; Dadmun, M.; Gurkan, B.; Tuckerman, M. E.; Maginn, E. J. Liquid Structure and Transport Properties of the Deep Eutectic Solvent Ethaline. *J. Phys. Chem. B* **2020**, *124*, 5251−5264.

(8) Wagle, D. V.; Deakyne, C. A.; Baker, G. A. Quantum chemical insight into the interactions and thermodynamics present in choline chloride based deep eutectic solvents. *J. Phys. Chem. B* **2016**, *120*, 6739−6746.

(9) Chatterjee, S.; Haldar, T.; Ghosh, D.; Bagchi, S. Electrostatic Manifestation of Micro-Heterogeneous Solvation Structures in Deep-Eutectic Solvents: A Spectroscopic Approach. *J. Phys. Chem. B* **2020**, *124*, 3709−3715.

(10) Stefanovic, R.; Ludwig, M.; Webber, G. B.; Atkin, R.; Page, A. J. Nanostructure, hydrogen bonding and rheology in choline chloride deep eutectic solvents as a function of the hydrogen bond donor. *Phys. Chem. Chem. Phys.* **2017**, *19*, 3297−3306.

(11) Kaur, S.; Kumari, M.; Kashyap, H. K. Microstructure of Deep Eutectic Solvents: Current Understanding and Challenges. *J. Phys. Chem. B* **2020**, *124*, 10601−10616.

(12) Nkuku, C. A.; LeSuer, R. J. Electrochemistry in Deep Eutectic Solvents. *J. Phys. Chem. B* **2007**, *111*, 13271−13277.

(13) Liao, H. G.; Jiang, Y. X.; Zhou, Z. Y.; Chen, S. P.; Sun, S. G. Shape-Controlled Synthesis of Gold Nanoparticles in Deep Eutectic Solvents for Studies of Structure−Functionality Relationships in Electrocatalysis. *Angew. Chem., Int. Ed.* **2008**, *47*, 9100−9103.

(14) Gutiérrez, M. C.; Ferrer, M. L.; Mateo, C. R.; del Monte, F. Freeze-Drying of Aqueous Solutions of Deep Eutectic Solvents: A Suitable Approach to Deep Eutectic Suspensions of Self-Assembled Structures. *Langmuir* **2009**, *25*, 5509−5515.

(15) Ferreira, E. S. C.; Voroshylova, I. V.; Figueiredo, N. M.; Cordeiro, M. N. D. S. Molecular dynamic study of alcohol-based deep eutectic solvents. *J. Chem. Phys.* **2021**, *155*, No. 064506.

(16) Faraone, A.; Wagle, D.; Baker, G.; Novak, E.; Ohl, M.; Reuter, D.; Lunkenheimer, P.; Loidl, A.; Mamontov, E. Glycerol hydrogen-bonding network dominates structure and collective dyanmics in a deep eutectic solvent. *J. Phys. Chem. B* **2018**, *122*, 1261−1267.

(17) Turner, A. H.; Holbrey, J. D. Investigation of glycerol hydrogen-bonding networks in choline chloride/glycerol eutectic-forming liquids using neutron diffraction. *Phys. Chem. Chem. Phys.* **2019**, *21*, 21782−21789.

(18) Mjalli, F. S.; Naser, J. Viscosity model for choline chloride-based deep eutectic solvents. *Asia-Pac. J. Chem. Eng.* **2015**, *10*, 273−281.

(19) Hossain, S. S.; Samanta, A. How do the hydrocarbon chain length and hydroxyl group position influence the solute dynamics in alcohol-based deep eutectic solvents? *Phys. Chem. Chem. Phys.* **2018**, *20*, 24613−24622.

(20) Fayer, M. D. Dynamics and structure of room temperature ionic liquids. *Chem. Phys. Lett.* **2014**, *616*−*617*, 259−274.

(21) Giammanco, C. H.; Yamada, S. A.; Kramer, P. L.; Tamimi, A.; Fayer, M. D. Structural and Rotational Dynamics of Carbon Dioxide in 1-Alkyl-3-methylimidazolium Bis(trifluoromethylsulfonyl)imide Ionic Liquids: The Effect of Chain Length. *J. Phys. Chem. B* **2016**, *120*, 6698−6711.

(22) Johnson, C. A.; Parker, A. W.; Donaldson, P. M.; Garrett-Roe, S. An ultrafast vibrational study of dynamical heterogeneity in the protic ionic liquid ethyl-ammonium nitrate. I. Room temperature dynamics. *J. Chem. Phys.* **2021**, *154*, No. 134502.

(23) Dinda, S.; Sil, A.; Das, A.; Tarif, E.; Biswas, R. Does urea modify microheterogeneous nature of ionic amide deep eutectics? Clues from non-reactive and reactive solute-centered dynamics. *J. Mol. Liq.* **2022**, *349*, No. 118126.

(24) Töpfer, K.; Pasti, A.; Das, A.; Salehi, S. M.; Vazquez-Salazar, L. I.; Rohrbach, D.; Feurer, T.; Hamm, P.; Meuwly, M. Structure, Organization, and Heterogeneity of Water-Containing Deep Eutectic Solvents. *J. Am. Chem. Soc.* **2022**, *144*, 14170−14180.

(25) Zhang, Q.; De Oliveira Vigier, K.; Royer, S.; Jérôme, F. Deep eutectic solvents: syntheses, properties and applications. *Chem. Soc. Rev.* **2012**, *41*, 7108−7146.

(26) Harifi-Mood, A. R.; Buchner, R. Density, viscosity, and conductivity of choline chloride plus ethylene glycol as a deep eutectic solvent and its binary mixtures with dimethyl sulfoxide. *J. Mol. Liq.* **2017**, *225*, 689−695.

(27) Kyungwon, K.; Daniel, E. R.; Fayer, M. D. Taking apart the two-dimensional infrared vibrational echo spectra: More information and elimination of distortions. *J. Chem. Phys.* **2008**, *128*, No. 204505.

(28) Kashid, S. M.; Jin, G. Y.; Chakrabarty, S.; Kim, Y. S.; Bagchi, S. Two-Dimensional Infrared Spectroscopy Reveals Cosolvent-Composition-Dependent Crossover in Intermolecular Hydrogen-Bond Dynamics. *J. Phys. Chem. Lett.* **2017**, *8*, 1604−1609.

(29) Kramer, P. L.; Nishida, J.; Giammanco, C. H.; Tamimi, A.; Fayer, M. D. Observation and Theory of Reorientation-Induced Spectral Diffusion in Polarization-Selective 2D IR Spectroscopy. *J. Chem. Phys.* **2015**, *142*, No. 184505.

(30) Cui, Y.; Fulfer, K. D.; Ma, J.; Weldeghiorghis, T. K.; Kuroda, D. G. Solvation Dynamics of an Ionic Probe in Choline Chloride-Based Deep Eutectic Solvents. *Phys. Chem. Chem. Phys.* **2016**, *18*, 31471−31479.

(31) Cui, Y.; Rushing, J. C.; Seifert, S.; Bedford, N. M.; Kuroda, D. G. Molecularly Heterogeneous Structure of a Nonionic Deep Eutectic Solvent Composed of N-Methylacetamide and Lauric Acid. *J. Phys. Chem. B* **2019**, *123*, 3984−3993.
(32) Yuan, R.; Fayer, M. D. Dynamics of Water Molecules and Ions in Concentrated Lithium Chloride Solutions Probed with Ultrafast 2D IR Spectroscopy. *J. Phys. Chem. B* **2019**, *123*, 7628−7639.
(33) Jadżyn, J.; Świergiel, J. The viscous consequence of different trends in clustering of 1,2-diol and 1,n-diol molecules. *Phys. Chem. Chem. Phys.* **2018**, *20*, 21640−21646.
(34) Szefczyk, B.; D S Cordeiro, M. N. Physical properties at the base for the development of an all-atom force field for ethylene glycol. *J. Phys. Chem. B* **2011**, *115*, 3013−3019.
(35) Li, C.; Zhang, J.; Zhang, T.; Wei, X.; Zhang, E.; Yang, N.; Zhao, N.; Su, M.; Zhou, H. Density, Viscosity, and Excess Properties for 1,2-Diaminoethane + 1,2-Ethanediol at (298.15, 303.15, and 308.15) K. *J. Chem. Eng. Data* **2010**, *55*, 4104−4107.
(36) Kyungwon, K.; Sungnam, P.; Ilya, J. F.; Fayer, M. D. Frequency-frequency correlation functions and apodization in two-dimensional infrared vibrational echo spectroscopy: A new approach. *J. Chem. Phys.* **2007**, *127*, No. 124503.
(37) Abraham, M. J.; Murtola, T.; Schulz, R.; Páll, S.; Smith, J. C.; Hess, B.; Lindahl, E. GROMACS: High performance molecular simulations through multi-level parallelism from laptops to supercomputers. *SoftwareX* **2015**, *1−2*, 19−25.
(38) Doherty, B.; Acevedo, O. OPLS Force Field for Choline Chloride-Based Deep Eutectic Solvents. *J. Phys. Chem. B* **2018**, *122*, 9982−9993.
(39) Wang, J.; Wolf, R. M.; Caldwell, J. W.; Kollman, P. A.; Case, D. A. Development and Testing of a General Amber Force Field. *J. Comput. Chem.* **2004**, *25*, 1157−1174.
(40) Brehm, M.; Thomas, M.; Gehrke, S.; Kirchner, B. TRAVIS—A free analyzer for trajectories from molecular simulation. *J. Chem. Phys.* **2020**, *152*, No. 164105.
(41) Deshmukh, S. H.; Chatterjee, S.; Ghosh, D.; Bagchi, S. Ligand Dynamics Time Scales Identify the Surface−Ligand Interactions in Thiocyanate-Capped Cadmium Sulfide Nanocrystals. *J. Phys. Chem. Lett.* **2022**, *13*, 3059−3065.
(42) King, J. T.; Ross, M. R.; Kubarych, K. J. Ultrafast α-Like Relaxation of a Fragile Glass-Forming Liquid Measured Using Two-Dimensional Infrared Spectroscopy. *Phys. Rev. Lett.* **2012**, *108*, No. 157401.
(43) Sun, Z.; Zhang, W.; Ji, M.; Hartsock, R.; Gaffney, K. J. Contact Ion Pair Formation between Hard Acids and Soft Bases in Aqueous Solutions Observed with 2DIR Spectroscopy. *J. Phys. Chem. B* **2013**, *117*, 15306−15312.
(44) Sakpal, S. S.; Deshmukh, S. H.; Chatterjee, S.; Ghosh, D.; Bagchi, S. Transition of a Deep Eutectic Solution to Aqueous Solution: A Dynamical Perspective of the Dissolved Solute. *J. Phys. Chem. Lett.* **2021**, *12*, 8784−8789.
(45) Youngren, G. K.; Acrivos, A. Rotational Friction Coefficients for Ellipsoids and Chemical Molecules with the Slip Boundary Condition. *J. Chem. Phys.* **1975**, *63*, No. 3846.
(46) Hu, C. M.; Zwanzig, R. Rotational friction coefficients for spheroids with the slipping boundary condition. *J. Chem. Phys.* **1974**, *60*, 4354−4357.
(47) Kaur, S.; Kashyap, H. K. Unusual Temperature Dependence of Nanoscale Structural Organization in Deep Eutectic Solvents. *J. Phys. Chem. B* **2018**, *122*, 5242−5250.
(48) Spittle, S.; Poe, D.; Doherty, B.; Kolodziej, C.; Heroux, L.; Haque, M. A.; Squire, H.; Cosby, T.; Zhang, Y.; Fraenza, C.; Bhattacharyya, S.; Tyagi, M.; Peng, J.; Elgammal, R. A.; Zawodzinski, T.; Tuckerman, M.; Greenbaum, S.; Gurkan, B.; Burda, C.; Dadmun, M.; Maginn, E. J.; Sangoro, J. Evolution of microscopic heterogeneity and dynamics in choline chloride-based deep eutectic solvents. *Nat. Commun.* **2022**, *13*, No. 219.
(49) Percevault, L.; Jani, A.; Sohier, T.; Noirez, L.; Paquin, L.; Gauffre, F.; Morineau, D. Do Deep Eutectic Solvents Form Uniform Mixtures Beyond Molecular Microheterogeneities? *J. Phys. Chem. B* **2020**, *124*, 9126−9135.

https://doi.org/10.1021/acs.jpcb.2c06521
J. Phys. Chem. B 2022, 126, 8331−8337